

Growth and properties of strained VO_x thin films with controlled stoichiometry

A. D. Rata¹, A. R. Chezan², and T. Hibma¹

¹*Chemical Physics, Materials Science Centre, Rijksuniversiteit Groningen,
Nijenborgh 4, Groningen 9747 AG, The Netherlands and*

²*Nuclear Solid State Physics, Materials Science Centre, Rijksuniversiteit Groningen,
Nijenborgh 4, Groningen 9747 AG, The Netherlands*

M. W. Haverkort, and L. H. Tjeng

II. Physikalisches Institut, Universität zu Köln, Zùlpicher Str. 77, 50937 Köln, Germany

H. H. Hsieh, H.-J. Lin and C. T. Chen

Synchrotron Radiation Research Center, Hsinchu 30077, Taiwan

(Dated: March 22, 2022)

We have succeeded in growing epitaxial films of rocksalt VO_x on $\text{MgO}(001)$ substrates. The oxygen content as a function of oxygen flux was determined using $^{18}\text{O}_2$ -RBS and the vanadium valence using XAS. The upper and lower stoichiometry limits found are similar to the ones known for bulk material ($0.8 < x < 1.3$). From the RHEED oscillation period a large number of vacancies for both vanadium and oxygen were deduced, i.e. $\approx 16\%$ for stoichiometric VO. These numbers are, surprisingly, very similar to those for bulk material and consequently quite strain-insensitive. XAS measurements reveal that the vacancies give rise to strong low symmetry ligand fields to be present. The electrical conductivity of the films is much lower than the conductivity of bulk samples which we attribute to a decrease in the direct overlap between t_{2g} orbitals in the coherently strained layers. The temperature dependence of the conductivity is consistent with a variable range hopping mechanism.

I. INTRODUCTION

One of the major challenges in transition-metal oxide thin film research is to grow the material in single crystal form with controlled oxygen stoichiometry. This is not a trivial task especially when the transition metal ion has multiple valences and the variation of the oxygen content leads to a rich and complex phase diagram. Important examples for such materials include the binary oxide systems like the vanadium and titanium oxides^{1–5}. The most common and convenient growth methods in thin film research like pulsed laser deposition and sputtering techniques are not very suitable here, because of the high substrate temperatures and consequently also high oxygen pressures usually used, giving less opportunity to fine tune the oxygen stoichiometry. These techniques are obviously the method of choice for ternary and quaternary oxides, in which one can vary the material properties by tuning one of the constituent cation concentrations while keeping that of the oxygen fixed. For the binary oxides, however, one has to resort to true molecular beam epitaxy (MBE) techniques, in which one has to carefully balance the oxygen flux with respect to the metal evaporation rates in order to obtain good control and tuning of the stoichiometry. The question here is whether one can obtain thin films with physical properties that are systematic, controllable and tunable.

Here we report on our research project to grow single crystal thin films of vanadium monoxide (VO_x), as well as on the study of the physical properties and the electronic structure of these films. Bulk vanadium monoxide has many intriguing properties that are closely related to

the issue of stoichiometry. While at first sight the crystal seems to have the very simple *fcc* rocksalt structure, it actually can have a very wide range of varying oxygen concentrations: values of $x = 0.8 - 1.3$ have been reported for bulk VO_x . Even more remarkable is that there is a large number of both cation and anion vacancies, even for $x = 1$, in which case the concentrations are as high as 15% ⁶. Stoichiometric VO always remains disordered, whereas ordering of the vacancies was only reported for x between 1.2 and 1.3⁷. A systematic investigation of the physical properties of polycrystalline VO_x has been carried out by Banus *et al.*⁶ in the early 70's. VO_x shows an interesting transition from a metallic to a semiconducting type of behavior at x close to 1, and the magnetic susceptibility can be described by a Curie-Weiss law, suggesting that the V *3d* electrons partially localize³. Several models have been proposed to explain these properties, in which the role of electron correlation effects, band formation and vacancies are discussed^{8–11}.

Only very little work on films of VO_x has been done up to now. Metal supported vanadium oxides were investigated by several authors in connection with catalytic properties. Thin V oxide layers deposited on $\text{Cu}(100)$ ^{12,13} and $\text{Ni}(110)$ ¹⁴ were found to consist of a V_2O_3 -like oxide phase after room temperature oxidation. VO_x -like islands growth was reported on $\text{Rh}(111)$ ¹⁵. Surnev *et al.* found a VO/VO_2 - like phase at low coverage on $\text{Pd}(111)$ using scanning tunnelling microscopy (STM)^{16,17}. Thin films of VO_x have also been grown on TiO_2 substrates, because of the enhanced catalytic activity shown by titania-supported vanadium oxides¹⁸. Sami *et al.*^{19–21} studied locally ordered VO_x films with a

thickness up to 4 ML grown on $\text{TiO}_2(110)$ by evaporating vanadium metal at room temperature and subsequent annealing in vacuum for a short period of time, in order to promote the uptake of oxygen from the substrate. From a structural point of view, local order of their films is supported by X-ray photoelectron diffraction (XPD).

In the examples mentioned above, the vanadium oxidation state was established on the basis of the position and shape of the $\text{V } 2p_{3/2}$ photoemission line. However, the uncertainty of stoichiometry of vanadia films remains, since the binding energies (BE) of $\text{V } 2p_{3/2}$ for different oxidation states are very close, a comparison between data obtained in Refs.¹² and¹⁹ showing some discrepancies. Moreover, a determination of the physical properties of VO_x thin films is missing in these studies. Preparation is often found to be difficult since VO_x easily oxidizes to V_2O_3 . These problems can be avoided by growing epitaxial films of VO_x on appropriate substrates with a careful optimization of the evaporation conditions.

This paper describes how we have been able to successfully grow coherent epitaxial single crystalline VO_x thin films by stabilizing them on $\text{MgO}(100)$ substrates. The paper is organized as follows. The details of the experimental conditions and equipment used are given in the experimental section (section II). The results are described in several subsections. We first present (section IIIA) the growth process as monitored structurally *in-situ* by reflection high-energy electron diffraction (RHEED) and low-energy electron diffraction (LEED) and compositionally by x-ray photoelectron spectroscopy (XPS). We then (section IIIB) determine the stoichiometry x of the various VO_x films by using Rutherford backscattering spectrometry (RBS). Further structural details of the epitaxy (section IIIC) is revealed by *ex-situ* x-ray diffraction (XRD). The important issue of vacancy concentrations is addressed using a combination of the RBS and RHEED intensity oscillations (section IIID). Basic data about the electronic structure, such as the valence and local crystal fields of the ions, (section IIIE) are measured using soft-x-ray absorption spectroscopy (XAS). We end the results section by presenting the temperature dependent transport properties of the films (section IIIF). Finally we discuss the results by comparing the properties of the VO_x thin films with those of the bulk material, and with the predictions made by existing theoretical models.

II. EXPERIMENTAL

The experiments were performed in an ultra-high vacuum (UHV) MBE system, with a base pressure below 1×10^{-10} mbar, equipped with RHEED, LEED and XPS facilities. RBS and XRD were used to characterize the thin films grown in the MBE system *ex-situ*. $\text{MgO}(100)$ was chosen as the substrate because it has the same cubic rocksalt structure as VO_x , with a mismatch of about 3%. MgO blocks were cleaved *ex-situ* and immedi-

ately introduced into the UHV chamber where the substrates were cleaned by annealing at 650°C for 2 hours in 1×10^{-6} mbar oxygen to remove hydrocarbon contaminations. Clean and well-ordered surfaces, as determined by XPS, RHEED and LEED were obtained. Vanadium (V) (purity 99.99%) was evaporated using an electron-beam evaporator (Omicron EFM3). The deposition rate of V, measured by moving a quartz crystal at the position of the substrate, was set to $0.7 - 0.8 \text{ \AA}/\text{min}$. The vanadium was simultaneously oxidized by a beam of $^{18}\text{O}_2$ (99.99%). The oxygen was supplied through a leak valve into a small buffer volume²² connected to the vacuum chamber through a 35 cm long and 1 cm wide stainless steel pipe, ending at a distance of 10 cm from the substrate. The pressure in the buffer volume was measured with a Baratron capacitance manometer. The variation in buffer pressure during deposition was less than 1%. VO_x films with different stoichiometries were grown by varying the $^{18}\text{O}_2$ buffer volume pressure, while keeping the V flux constant. During evaporation the background pressure was 2×10^{-8} mbar or lower. The V and $^{18}\text{O}_2$ beams can be abruptly and simultaneously stopped. After closing the $^{18}\text{O}_2$ valve the background pressure dropped to below 10^{-9} mbar within seconds, insuring a well-defined oxygen exposure of the sample. All the samples were grown while keeping the substrate at room temperature (RT).

RHEED was used to monitor the evolution of the films. Thicknesses were calibrated by monitoring the RHEED intensity oscillations during deposition. Oscillations in the RHEED specular beam intensity, where each oscillation corresponds to the formation of one new atomic monolayer (ML), allows for control of the film thickness. Film thicknesses were also determined *ex-situ* from X-ray specular reflectivity (XRR) measurements^{23,24} and a good agreement with RHEED intensity oscillations was obtained.

XPS measurements were performed using non-monochromatic Al $K\alpha$ radiation ($h\nu = 486.6 \text{ eV}$) and the total energy resolution of the electron analyzer in combination with the photon source is about 1 eV. To avoid *ex-situ* post-oxidation, a thin MgO cap layer (20 Å) was grown for protection by Mg deposition in $^{18}\text{O}_2$ atmosphere of 1×10^{-8} mbar at room temperature. Consequently all the *ex-situ* measurements, i.e. RBS, XRD, XAS and electrical measurements were done on capped VO_x samples.

To determine the oxygen content, RBS measurements have been performed. For calibration purposes a V_2O_3 epitaxial thin film was also grown on an $\text{Al}_2\text{O}_3(0001)$ substrate, with the oxygen partial pressure and the substrate temperature set at 10^{-6} mbar and 550°C respectively²⁵⁻²⁷. All the measurements were done in a so-called 'random' orientation with respect to the crystalline axes, using a He^+ beam with 1.5 MeV energy. The backscattering yields were detected at an angle of 165° degrees.

The XRD measurements were done using a Philips

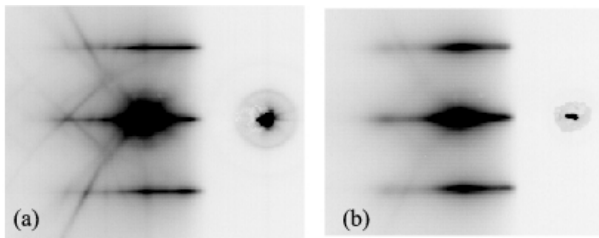


FIG. 1: RHEED patterns recorded at an electron energy of 15 kV with the beam incident along [100] direction. (a) clean MgO(100) substrate. (b) 20 Å VO_x (100) thin film grown on MgO(100) substrate using 0.18 mTorr oxygen buffer pressure while keeping the substrate at room temperature. The picture is inverted in order to observe better the Kikuchi lines.

MRD diffractometer, equipped with a hybrid mirror/monochromator for Cu K_α radiation, a 4-circle goniometer and a programmable slit in front of the detector.

The X-ray absorption spectroscopy (XAS) measurements were performed at the 11A Dragon beamline^{28,29} at the Synchrotron Radiation Research Center Taiwan, using the total electron yield mode. The light has a degree of linear polarization of 98% and an energy resolution of 0.16 eV for photon energies between 500 and 550 eV. The spectra are normalized to the photon flux measured using a gold mesh. The angle of the incident light is normal to the VO_x films.

Resistivity measurements were performed in a commercial Quantum design PPMS system. The electrical measurements were done in the constant voltage mode and the current was measured along the [100] direction of the films by two and four point geometry. Electrical contacts consisting of 10 nm of Cr metal were evaporated *ex-situ* on the MgO substrates prior to introduction into the MBE system, in order to measure the resistance of as-grown VO_x films.

III. RESULTS

A. Growth of VO_x thin films

For a wide range of incident oxygen fluxes, epitaxial growth of VO_x thin films on MgO(100) substrates was concluded from *in situ* RHEED and LEED analysis. Our MBE system geometry allows for monitoring changes in surface structure during film growth by RHEED. This low angle electron diffraction technique is particularly suited to thin film growth as it is highly sensitive to surface morphology. A RHEED pattern of a clean MgO(100) surface and 20 Å thick VO_x thin film deposited on MgO(100) is shown in Fig.1.

The beam was incident along the [100] direction. The basic RHEED pattern did not change during growth, suggesting that the film continues to grow as a rocksalt phase on top of the underlying substrate. Sharp streaks and the presence of Kikuchi lines indicate that the surface is still

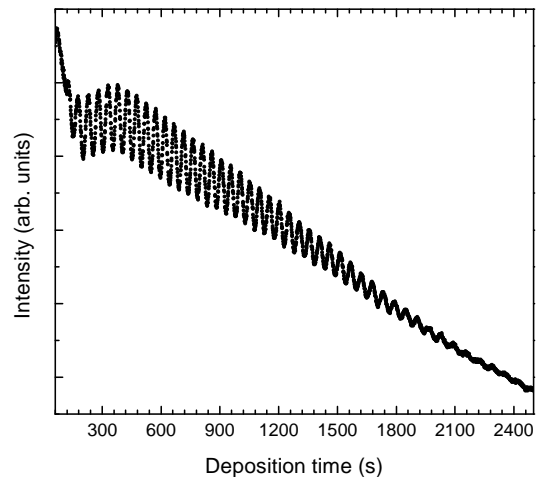


FIG. 2: RHEED intensity oscillations of the specularly reflected electron beam observed during deposition of VO_x on MgO(100). The electron beam was incident along the [100] direction, with a primary energy of 15 kV.

smooth after deposition of 10 monolayers (ML) of VO_x .

In most cases oscillations in the intensity of the specularly reflected beam were observed during growth. These oscillations are characteristic for a *layer-by-layer* growth mode, each oscillation corresponding to the formation of one atomic layer. Note that RHEED oscillations were observed at room temperature, which is considered to be a very low temperature for an oxide system. In Fig.2 an example of these growth oscillations is shown.

In Fig.3 a sequence of RHEED patterns which were taken after deposition of about 50 monolayers of VO_x using different oxygen fluxes is presented.

The oxygen content x is indicated on each RHEED pattern. The corresponding oxygen flux used can be found in the caption of Fig.3. In paragraph III.B we will explain how the x values were determined using RBS spectrometry. Varying the oxygen buffer pressure between 0.12 and 0.20 mTorr ($0.82 < x < 0.97$) epitaxial growth is obtained and sharp streaks can still be observed after deposition of 50 ML VO_x . The distance between VO_x streaks is the same as between the MgO streaks. This is consistent with a coherent growth as determined *ex-situ* by XRD, which will be discussed in section III.C. The rocksalt structure of VO_x thin films was also confirmed by LEED. The LEED pattern displays the same square symmetry and periodicity as a MgO(100) surface.

Between 0.22 and 0.30 mTorr ($1.1 < x < 1.31$), MgO RHEED streaks fade away quickly after starting the growth and 3D-transmission spots appear, suggesting considerable roughening of the surface. The absence of a LEED pattern for the $x = 1.28$ and $x = 1.31$ cases confirms that the surface morphology is becoming increasingly disordered. Nevertheless, the presence of RHEED oscillations shows that the growth is still *layer-by-layer* like.

For an oxygen buffer pressure of less than 0.12 mTorr

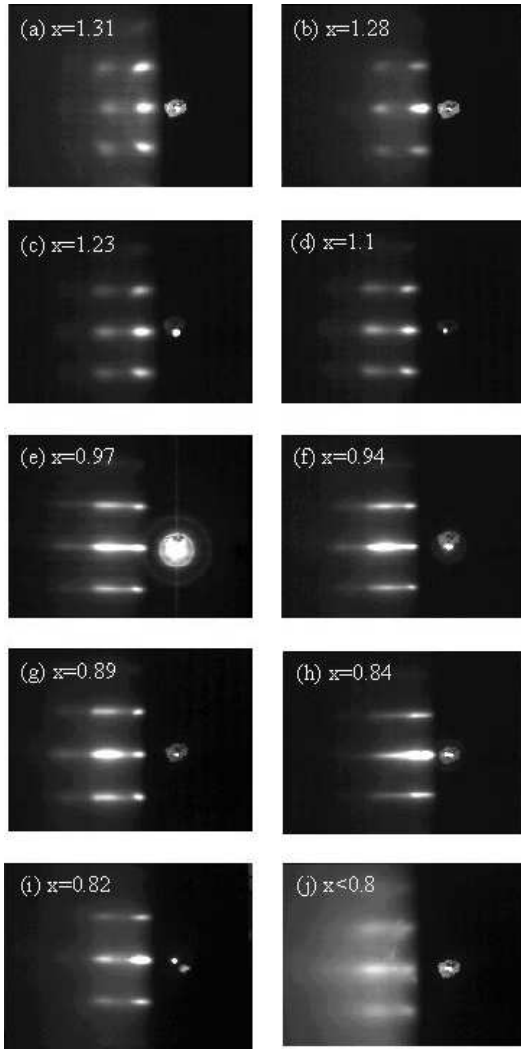


FIG. 3: Sequence of RHEED patterns observed after deposition of 50 ML VO_x on $\text{MgO}(100)$ at different oxygen fluxes while keeping the substrate at room temperature. The oxygen buffer pressure was varied between 0.10 and 0.30 mTorr: (a) 0.30 mTorr, (b) 0.27 mTorr, (c) 0.24 mTorr (d) 0.22 mTorr, (e) 0.20 mTorr, (f) 0.18 mTorr, (g) 0.16 mTorr, (h) 0.14 mTorr, (i) 0.12 mTorr, (j) 0.10 mTorr. The electron beam was incident along $[100]$ direction, with a primary energy of 15 kV.

($x < 0.8$) powder rings and extra spots were observed in RHEED. Vanadium atoms were not completely oxidized in the later case as deduced from XPS core level intensities.

Attempts to make VO_x films at higher substrate temperature were unsuccessful. The RHEED pattern quickly disappeared or was getting very diffuse from the beginning.

The V-2*p* and O-1*s* core lines measured for three different films i.e vanadium metal on $\text{MgO}(100)$, VO_x on $\text{MgO}(100)$ and V_2O_3 on $\text{Al}_2\text{O}_3(0001)$ are shown in Fig.4. The binding energies were corrected for the charging effect by assuming a constant binding energy of the O 1*s*

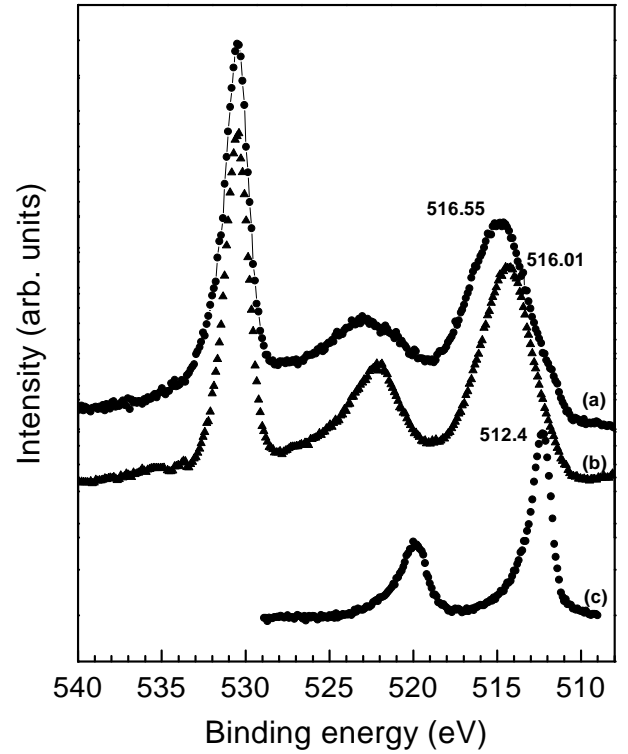


FIG. 4: V 2*p* and O 1*s* XPS spectra of (a) V_2O_3 on $\text{Al}_2\text{O}_3(0001)$, (b) VO_x on $\text{MgO}(001)$ and (c) vanadium metal on $\text{MgO}(001)$.

peak at 531 eV. All spectra were corrected in a standard manner for the satellites due to the $\text{K}\alpha_3\alpha_4$ components of the incident X-ray and an integral background was subtracted afterwards. The binding energies of the V 2*p*_{3/2} peak found are given in the figure. The binding energy corresponding to the V 2*p*_{3/2} in the VO_x film was found between the ones corresponding to V metal and V_2O_3 , respectively (see Fig.4). The vanadium oxidation state can be in principle determined from the position and shape of the V 2*p*_{3/2} feature. Nevertheless, due to the fact that vanadium with different oxidation states has rather similar values for the binding energies³⁰ we did not perform a quantitative analysis of the XPS data. In order to determine precisely the stoichiometry we have adopted a different route, which will be presented in the following section.

B. Stoichiometry determination

The oxygen content of the films was determined from RBS measurements. As was mentioned already in the experimental part, $^{18}\text{O}_2$ instead of $^{16}\text{O}_2$ was employed for film growth to distinguish between the oxygen of the film and substrate. Using a 1.5 MeV He^+ beam, a good mass separation between ^{16}O from the substrate and ^{18}O from the film can be obtained. This can be observed in Fig.5 showing a RBS spectrum of a V_2O_3 layer grown

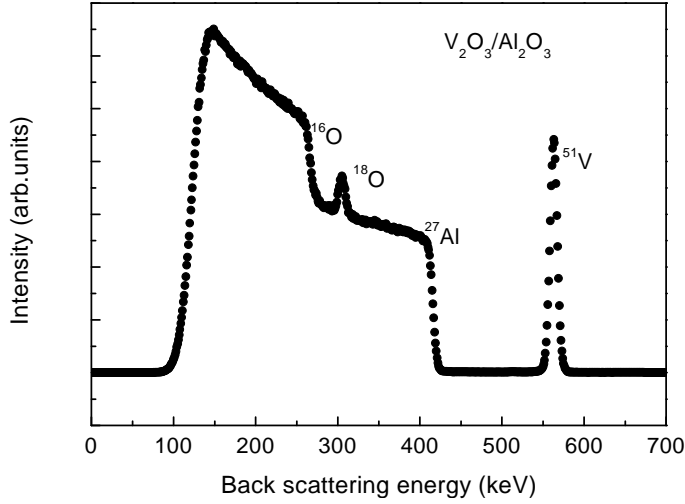


FIG. 5: RBS spectra of 1.5 MeV He^+ ions scattered from a V_2O_3 film epitaxial grown on an $\text{Al}_2\text{O}_3(0001)$ substrate. The ^{18}O peak can be clearly distinguished.

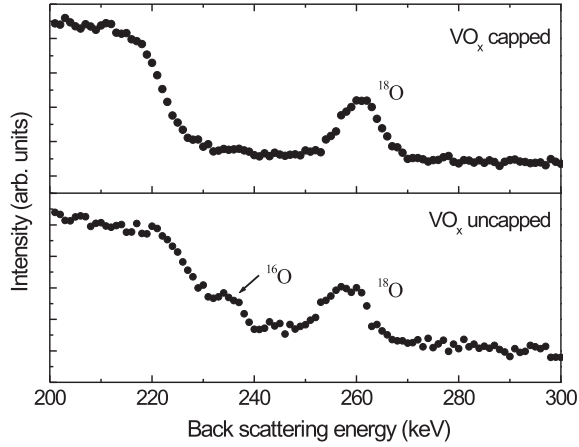


FIG. 6: RBS spectra of 1.5 MeV He^+ ions scattered from VO_x film deposited on $\text{MgO}(100)$. (a) with a thin (2nm) MgO caplayer, (b) without caplayer. An extra shoulder at the ^{16}O position is observed due to postoxidation.

epitaxially on an $\text{Al}_2\text{O}_3(0001)$ substrate, which was used for calibration. A nice hexagonal LEED pattern characteristic for the corundum structure was observed, proving the high quality and long range order of the V_2O_3 film. In Fig.6 part of the spectra for a capped and uncapped VO_x layer on $\text{MgO}(001)$ is shown. In both spectra a well-separated ^{18}O -peak is visible. For the uncapped layer, an additional shoulder at the ^{16}O position can be observed due to the fact that the layer is post-oxidized in air. The absence of this shoulder in the spectrum of the capped layer proves that capped VO_x films are really protected from post-oxidation.

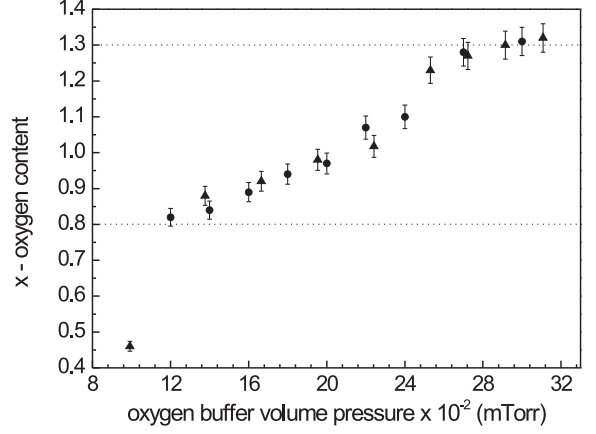


FIG. 7: The oxygen content x as a function of the buffer volume pressure as determined from RBS data for two series of VO_x samples.

With the following formula we have calculated the ratio between the numbers of V and O atoms in a VO_x film, using V_2O_3 as a reference sample.

$$x = \frac{3 \left[\frac{A_O}{A_V} \right]_{\text{VO}_x}}{2 \left[\frac{A_O}{A_V} \right]_{\text{V}_2\text{O}_3}} \quad (1)$$

The areas A_O and A_V in the RBS spectra were determined by fitting the V and ^{18}O peaks from VO_x and V_2O_3 samples to a gaussian function, in the case of the ^{18}O -peak after subtraction of the linear background due to Mg. The ^{18}O -peak area was corrected for the contribution of the caplayer, using the thickness of the VO_x films and the Mg^{18}O caplayer, as determined from the RHEED oscillations. The resulting x -values are plotted in Fig.7 as a function of the oxygen buffer volume pressure for two series of samples. One can observe that the x values are nicely reproducible. The error in the determination is about 3%. The upper and lower stoichiometry limit found are similar to the ones known for bulk material. For the sample grown at 0.10 mTorr the vanadium metal is not completely oxidized, as deduced from the XPS spectra. For x bigger than 1.3 a mixture of two phases was found.

C. Structure of VO_x thin films

From RHEED and LEED patterns it was already concluded that VO_x films grow epitaxially on $\text{MgO}(100)$. To analyze the epitaxy and crystal structure of the films in a more quantitative way, we also performed an *ex-situ* XRD analysis.

The measurements were done on samples capped with a thin (20Å) epitaxial MgO film. θ - 2θ scans show only

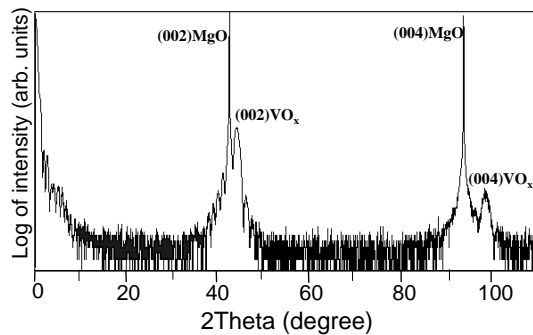


FIG. 8: θ - 2θ X-ray diffraction measurement of 10nm thick VO_x thin film prepared with $x = 0.94$. Only the (002) and (004) diffraction peaks characteristic of the rocksalt structure can be observed. The reflections from the film are broadened due to the finite thickness of the film. Subsidiary thickness fringes indicate a well defined composition and thickness of the film.

weak diffraction peaks close to the (002) and (004) peaks of the MgO substrate, as expected from films having a rocksalt structure. The reflections are broadened due to the finite thickness of the film. There are no peaks corresponding to other phases. Moreover, for samples made with the oxygen buffer pressure varying between 0.12 and 0.22 mTorr a number of subsidiary thickness fringes were observed, suggesting a well defined composition and thickness of the film (see Fig.8).

To determine whether the growth is fully coherent or partially relaxed, the most convenient way is to measure the intensity profile around a non-specular reflection common to the substrate and the overlayer. This can be done by performing a set of 2θ - ω scans at different ω , 2θ and ω being the detector and sample orientations with respect to the beam direction. These scans can be easily mapped into reciprocal space. An example of such a map for the region in reciprocal space around the (113) reflection is shown in Fig.9. The horizontal and vertical axes are k vectors parallel (k_{par}) and perpendicular (k_{per}) to the surface plane, respectively. The intensity scale in the figure is logarithmic. The feature corresponding to the VO_x film can be clearly distinguished. The elongated shape of the MgO reflection perpendicular to the radial direction is due to mosaic spread. The peaks of MgO and VO_x are at the same k_{par} value, which proves that the film is fully coherent. Consequently, VO_x thin films experience a compressive strain in the perpendicular direction, which is induced by the lattice mismatch.

The lattice constant normal to the substrate surface can be determined from $\theta - 2\theta$ scans around MgO(002) or MgO(004) peaks using the Bragg law. 2θ values were determined by fitting the peaks to a gaussian function. The perpendicular lattice constant is plotted in Fig.10 as a function of the oxygen content.

We found that the perpendicular lattice constant and consequently also the average lattice constant is decreasing with increasing oxygen content. This is in contrast

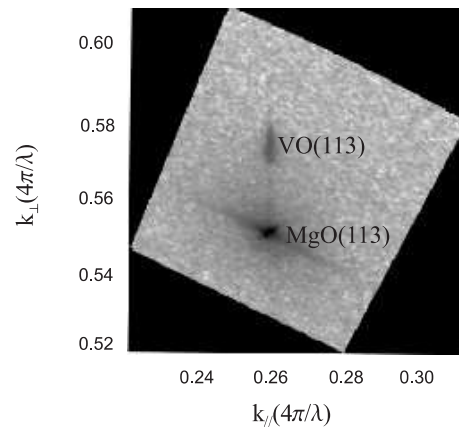


FIG. 9: XRD map of reciprocal space around the non-specular (113) reflection of a 10nm thick VO_x thin film with $x = 0.94$. The logarithm of the diffracted intensity as a function of the in-plane k_{\parallel} and out-of-plane k_{\perp} reciprocal lattice vectors is plotted. The x - and y - axis are in units of $\frac{4\pi}{\lambda}$, with $\lambda = 0.15015$ nm.

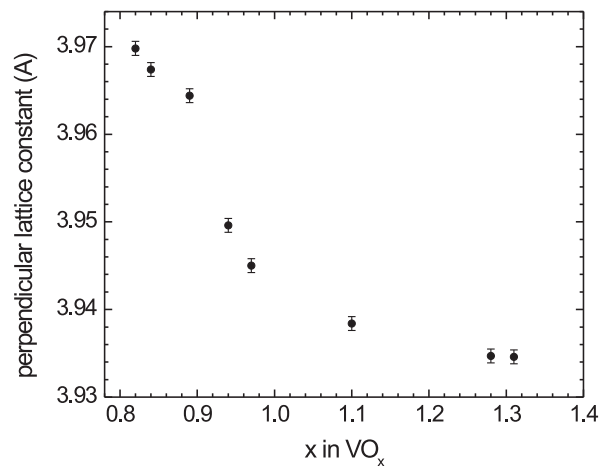


FIG. 10: Perpendicular lattice constant of VO_x films with different oxygen content as a function of x as determined from XRD. The perpendicular lattice constant is decreasing with increasing x .

to the behavior reported by Banus⁶ for bulk VO_x .

The layer thicknesses determined from X-ray specular reflectivity (XRR) measurements were in good agreement with the values obtained from the RHEED intensity oscillation period.

D. Vacancy concentration

As was already mentioned in the Introduction, a large number of both vanadium and oxygen vacancies is characteristic for bulk VO_x . Using a combination of RHEED

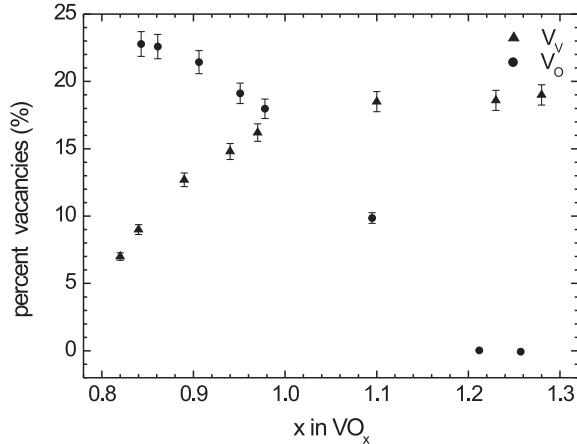


FIG. 11: Vanadium and oxygen vacancy concentrations in VO_x as determined from the period of RHEED oscillations. The number of vanadium vacancies is increasing with x , while the number of oxygen vacancies is decreasing.

and RBS results, an estimation of the number of vacancies present in VO_x thin films can be made. RHEED oscillation periods were determined for all the VO_x samples as well as for a calibration V_2O_3 thin film on $\text{Al}_2\text{O}_3(0001)$. All samples were grown using the same value for the vanadium flux. By comparing the time needed to grow one monolayer of VO_x and V_2O_3 and assuming that V_2O_3 is stoichiometric and free of vacancies, the fraction of vacant vanadium sites (V_V) in VO_x can be directly calculated. The oxygen vacancy concentration (V_O) can be obtained because x is already known from RBS, using the following expression:

$$x = \frac{1 - V_O}{1 - V_V} \quad (2)$$

As illustrated in Fig.11, the vanadium vacancy concentration is increasing with increasing oxygen content x , while the oxygen vacancy concentration is decreasing. The total number of vacancies ($V_V + V_O$) is also decreasing with x . Close to the stoichiometric value we found about 16 % vacant sites of both vanadium and oxygen.

E. Valence of the V ions from XAS

XAS measurements were done at the O K - edge in order to verify the valence of the V and O ions. The data are depicted in Fig.12 for samples with the oxygen content x (as determined from RBS) between 0.8 and 1.3. For comparison, we have also included the spectrum of a V_2O_3 film in top part of the figure. The O K -edge absorption spectra correspond to the dipole-allowed

transitions from the O $1s$ to the O $2p$ shell, which is partially empty due to the hybridization with V $3d$ conduction band states. The spectral structures that can be observed in the 528 – 534 eV photon energy range are dictated by these V $3d$ states^{31–34}. For photon energies higher than 535 eV, the oxygen of the MgO cap layer also start to contribute to the XAS signal³⁴.

The distinct peak observed at photon energies around 532 eV, can be assigned to transitions into the empty V $3d-e_g^\uparrow$ band³³. Structures at higher photon energies can be ascribed to transitions to the higher lying V $4sp$ related bands. Important is to note that for the most oxygen deficient VO_x samples, i.e. $x \ll 1$, the lowest spectral structure is given by the 532 eV peak, indicating that the lower lying V $3d-t_{2g}^\uparrow$ band is completely occupied by three electrons, and that thus the V valence is 2+ or less. For samples with higher oxygen content, i.e. for $x > 1$, a clear low energy peak appears at about 530 eV. This strongly suggests that holes are introduced in the V $3d-t_{2g}^\uparrow$ band, meaning that the V valence is higher than 2+. This assignment is supported by the V_2O_3 spectrum, in which transitions to both the t_{2g}^\uparrow and the e_g^\uparrow bands are possible because only two electrons occupy the three-fold degenerate t_{2g}^\uparrow orbital in this $\text{V}^{3+} 3d^2$ system.

These XAS measurements show that the cross-over from less than 2+ to more than 2+ V valencies occurs for an RBS x value of about 0.94 – 0.97. This value is not very far from 1.00, and can be taken as an indication for a good agreement between the XAS and RBS methods.

We have also carried out XAS experiments at the V $L_{23}(2p \rightarrow 3d)$ edges. The results are shown in Fig.13, in which we have also included the spectra for V_2O_3 and Cr_2O_3 for reference purposes. In going from $x = 0.8$ to $x = 1.3$ we can observe a gradual change in the spectra. Distinct and sharp structures start to develop for $x \geq 1$. The similarity of these structures with those of V_2O_3 is striking, and in fact indicates that V ions in a 3+ valence state are present for $x \geq 1$, consistent with the observations at the O K edge mentioned above.

Important is the observation that the spectra are quite broad for x around 1. In the simplest approximation, one would expect to see a spectrum with the typical atomic multiplet structure of a $2p^6 3d^3 \rightarrow 2p^5 3d^4$ transition of a V^{2+} ion in a O_H symmetry, as shown in the bottom curve of Fig.13. This curve has been calculated using standard parameters ($10D_q \simeq 2$ eV) often applied for the analysis of transition metal oxide soft-x-ray absorption spectra^{35–37} and it shows quite distinct features with several peaks and valleys. Clearly, the experimental V L_{23} spectra for $x \approx 1$ do not have these distinct features.

Also a comparison with the experimental spectrum of Cr_2O_3 (see Fig.13), which is also a $3d^3$ ion in approximately O_H local symmetry, leads to the conclusion that the V L_{23} spectra are anomalously broad. We take this observation as an indication that the vanadium in VO is not all in the local $3d^3 - O_H$ symmetry, but that instead an appreciable amount of vanadium ions are experiencing strong local ligand fields of low symmetry associated

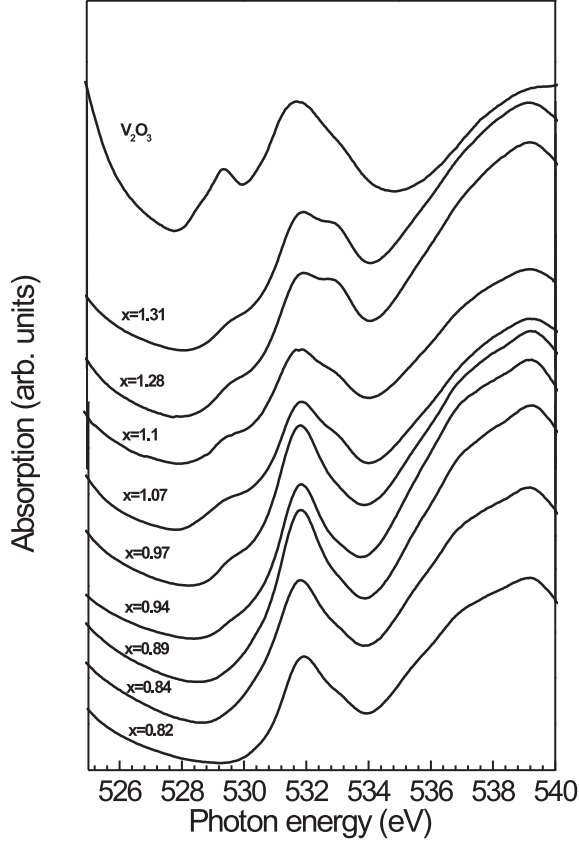


FIG. 12: O 1s X-ray absorption spectra of VO_x samples with the oxygen content varying between 0.8 and 1.3.

with the presence of large amount of vacancies. The low symmetry ligand fields must be at least several hundreds of meV strong, in order to wash out completely the multiplet structure of a $3d^3$ -ion in O_H symmetry. The implication of such fields will be discussed in Section IV.

F. Transport properties

Electrical measurements have been performed to study the electronic structure of VO_x films. Resistivity data have been reported previously by Banus⁶ for polycrystalline samples. Bulk material exhibits a semiconducting behavior for $x > 1$, with an activation energy rising to about 40 meV for $x = 1.3$. For $x < 1$ VO_x behaves like TiO_x , with an almost temperature and composition independent resistivity of about $3 \times 10^{-3} \Omega\text{cm}$. Banus et al. reported a transition from a semimetallic to semiconducting type behavior in VO_x at $x = 1.05$.

The variation of the logarithm of the electrical resistivity of VO_x thin films with different oxygen content is shown as a function of $1/T$ in Fig.14. The resistivity is increasing with decreasing T for all but the $x = 0.82$ sam-

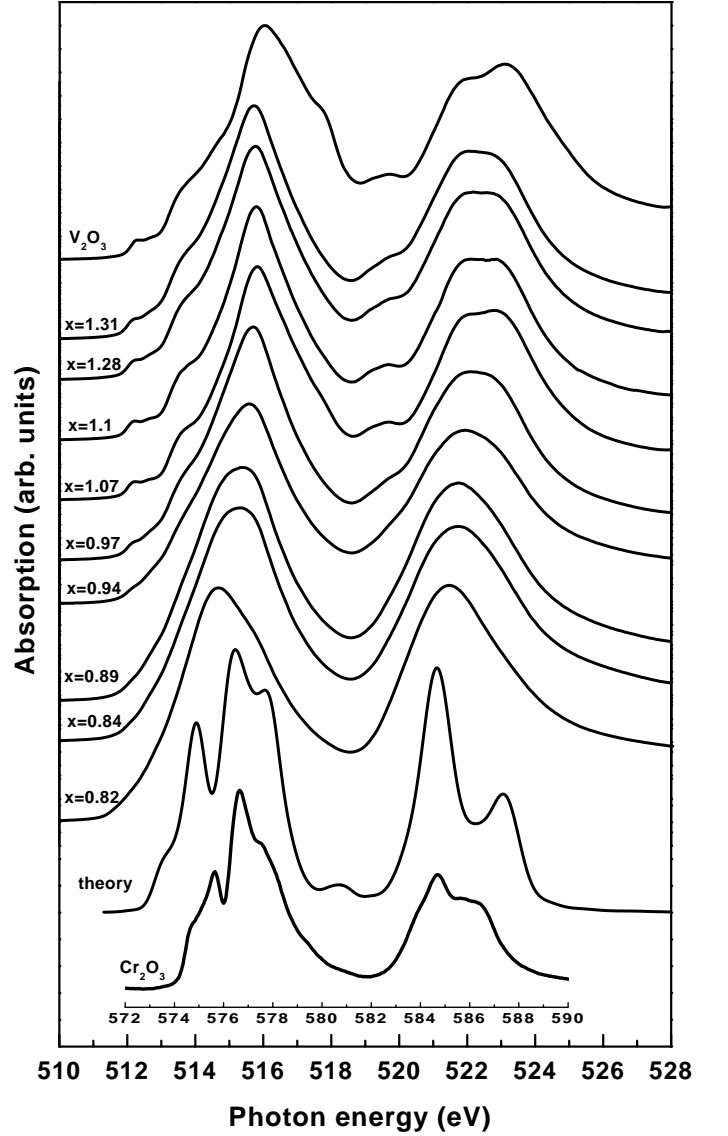


FIG. 13: V L_{23} X-ray absorption spectra of VO_x samples with the oxygen content varying between 0.8 and 1.3.

ple, suggesting a semiconductor-like behavior in the entire temperature range studied. However, it is evident in Fig.14 that $\log \rho$ does not vary linearly with $1/T$. Fig.15 shows the composition dependence of the activation energies calculated from the $\log \rho$ -vs- $1/T$ plots close to room temperature. Note, that the apparent activation energy decreases with decreasing temperature.

Such behavior is similar to that described by Banus⁶, but we did observe a few important differences. Compared to the corresponding resistivity results for bulk samples we found a much higher absolute value of the resistivity. As can be observed from Fig.14 the transition from a metallic to a semiconductor type behavior is shifted from $x = 1$, as found in bulk material, to $x = 0.8$ for thin films. Moreover, the activation energy calculated close to room temperature (Fig.15) is larger. For exam-

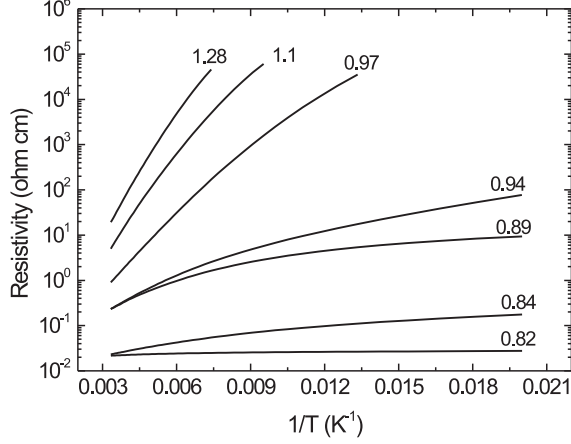


FIG. 14: Logarithm of resistivity of VO_x films with different oxygen content plotted against $1/T$. Resistivity is increasing with decreasing temperature except for the $x = 0.82$ sample, suggesting a semiconductor-like behavior.

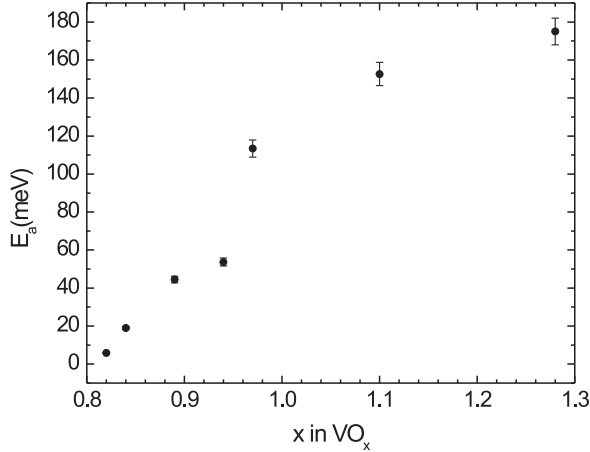


FIG. 15: Activation energy E_a versus x calculated for the temperature interval $150 < T < 300$ K.

ple, for bulk stoichiometric VO, Banus et al.⁶ obtained an apparent activation energy of only 5 meV. For thin films we found a much higher value of ≈ 110 meV. A large increase in the activation energy can be observed going from $x = 0.94$ to $x = 0.97$. Although the oxygen content is changing only with 3%, the activation energy is becoming almost twice as large. For $x \approx 1.3$ the activation energy rises to 180 meV.

The T-dependence of the resistivity is better described by variable range hopping behavior³⁸ given by:

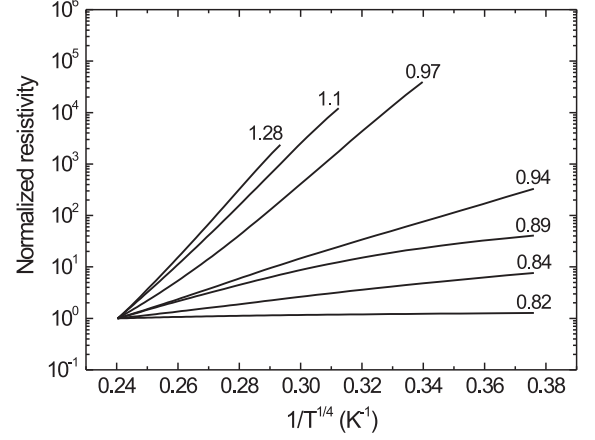


FIG. 16: Logarithm of normalized resistivity of VO_x thin films with different oxygen content plotted as a function of $T^{-1/4}$.

TABLE I: Parameters extracted from $T^{-1/4}$ dependence of resistivity.

x in VO_x	T_0 (K)	$N(E_F)$ ($\text{cm}^{-3}\text{eV}^{-1}$)
0.82	2.6	2×10^{26}
0.84	2×10^3	2×10^{23}
0.89	5×10^4	8×10^{21}
0.94	12×10^4	3×10^{21}
0.97	5×10^6	1×10^{20}
1.1	1×10^7	4×10^{19}
1.28	2×10^7	2×10^{19}

$$\rho \approx \exp\left(\frac{T_0}{T}\right)^{\frac{1}{4}} \quad (3)$$

This is evident from Fig.16 showing the normalized resistivity versus $T^{-1/4}$. This result is not surprising knowing that a high number of vacancies is characteristic for this material. A random field caused by vacant sites can produce localization of the electrons near the Fermi level just like in amorphous materials. Its occurrence in VO_x seems to be strong evidence that the vacancies play a major role, causing large changes in its electronic properties. The parameter T_0 can be extracted from the slope of the curves in Fig.16. T_0 is related to the density of localized states at the Fermi level $N(E_F)$ ³⁹ by the following expression:

$$T_0 = \frac{24\alpha^3}{\pi N(E_F)k_B} \quad (4)$$

where α^{-1} is the decay length of the wave function associated with the charge carriers and k_B is the Boltzmann constant. Taking a reasonable value for α^{-1} as 5 Å,

$N(E_F)$ can be calculated from the values of T_0 . These parameters are tabulated in Table 1 together with the corresponding x values. Clearly, one can observe that for $x = 0.82$ sample the density of localized states at the Fermi level is high and starts to decrease with increasing the oxygen content.

IV. DISCUSSION

The transport properties of VO_x can not be understood on the basis of a simple band picture, because the material should have been metallic. Shortly after the publication of Banus et al., two papers by Goodenough⁸ and Mott⁹ appeared, in which explanations were given in terms of electron correlation effects and vacancies. Both authors assume a finite Hubbard U , which is large enough to split the t_{2g} band. Because V^{2+} supplies 3 electrons to the t_{2g} band, the valence band of VO is given by a completely filled lower Hubbard band, separated by a gap from the conduction band which is the empty upper Hubbard band.

According to Mott⁹, the random field produced by the vacancies causes Anderson localization⁴⁰ in the overlap region of the two Hubbard bands. This explains why the conductivity in VO_x is of the variable range hopping type at low temperatures. In Goodenough's model⁸ the effect of the vacancies on the electronic structure is discussed much more explicitly. He assumes a high degree of trapping of electron and holes near anion and cation vacancies, respectively. In this way the Fermi-level stays near the minimum in the DOS of VO_x , explaining its semiconductor-like behavior. The transition to a more itinerant behavior for $x < 1$ is attributed to a tail in the trapped electron distribution. A second effect of the trapping of charges near vacancies is that the loss of Madelung energy is limited.

The presence of a large number of vacancies in VO_x remains one of the most puzzling characteristics. The only two other binary oxides showing this behavior are the rocksalts TiO_x and NbO , with NbO having about 25% vacancies⁴¹. Apparently the creation of vacancies stabilizes the crystal by reducing the Gibbs free energy. According to Goodenough⁸ the formation of vacancies leads to a reduction in the lattice constant, thereby broadening the t_{2g} bands. The resulting stabilization of the occupied valence band states is counteracted by a reduction in Madelung energy, but this energy loss is assumed to be minimized by a localization of the charge compensating electrons and holes near the oxygen and vanadium vacancies respectively. He argues that the application of hydrostatic pressure should reduce the vacancy concentration considerably and he refers to experiments giving indirect evidence in favor of this effect⁴².

The VO_x films we have grown epitaxially on MgO substrates are thin enough to be coherent with the substrate and are under tensile stress. In fact, the in-plane lattice constant is expanded ($\approx 3\%$), while the out-of-plane

lattice constant is reduced due to the Poisson effect. Applying Goodenough's vacancy induced lattice contraction arguments, we would expect that the formation of vacancies will not be less favored in our thin film, because the lattice constant of the film is fixed by the substrate, thus preventing the energy gain to occur that otherwise is associated with the lattice contraction and broadening of the t_{2g} bands. In contrast to this expectation, however, we found that both the cation and anion concentration are not much affected. For stoichiometric VO film, the values are even slightly higher (of the order of 1 or 2%) than for bulk material.

We agree with Goodenough, nevertheless, that the mechanism for vacancy formation must be searched for in terms of energy arguments. To our knowledge, *ab-initio* total energy calculations have not yet been carried out to study the stability of vacancy formation in this material. We may speculate about the mechanism by reviewing Goodenough's arguments⁸. Goodenough starts with the picture that electrons and holes are being trapped near the cation and anion vacancies, as to avoid part of the Madelung energy loss. The t_{2g} orbitals of cations neighboring a cation vacancy are then destabilized by a reduced bonding to neighboring t_{2g} orbitals and a stronger π bonding to the p orbitals next to the vacancy, thereby raising their energy above the Fermi level. On the other hand, near an oxygen vacancy the bonding t_{2g} orbitals are stabilized, whereas the e_g and s orbitals are less destabilized by the absence of oxygen p_σ orbitals at the vacant site. These effects contribute to the stabilization energy of vacancies, but not enough. Instead of looking for a possible further energy gain in the t_{2g} band due to lattice contraction induced band broadening, we now discuss what low symmetry ligand fields can do to lower the energy of the occupied t_{2g} , motivated by the fact that the XAS measurements reveal that those ligand fields are very strong in VO_x , i.e. with a strength of the order of several hundreds meV.

We will first discuss the case of oxygen vacancies. Neighboring divalent $3d$ metal ions are surrounded by five oxygen ligands in a square pyramidal arrangement with C_{4v} symmetry. The t_{2g} and e_g levels will be split into three non- and one doubly degenerate levels, respectively. With two electrons being trapped at or near the vacancy, we have one extreme possibility in that both electrons are trapped at the vacant site, forming an F -center, and the other possibility in that the excess electrons are trapped at neighboring d -metal sites. Assuming that at least a fraction of the excess electrons resides at the d -metal ions, the average number of d electrons will be larger than three for V-ions next to a vacancy. In both cases some ligand field stabilization energy is gained, owing to the electrons occupying the lower e_g level in $\text{VO}_{x<1}$.

Considering now the case of d metal vacancies, we may speculate that two excess holes are trapped near these vacancies in $\text{VO}_{x>1}$. One extreme possibility is that the holes are residing at oxygen neighbors. Following a suggestion of Elfimov et al.⁴³, this would give a stable config-

uration in which the holes are in a triplet state localized at the oxygen coordination polyhedron around the vacancy. However, in contrast to the case of CaO discussed by these authors, in a transition metal compound there is also the possibility that the two holes are located at next nearest neighbor transition metal ions. The presence of the cation vacancy leads to a local symmetry lowering (C_{2v}) at these cation sites. Also in this case a ligand field stabilization is anticipated, because the average number of d electrons on d -metal ions next to a vacancy will be less than three for V.

Although, as was argued above, the decrease of direct overlap between t_{2g} orbitals in the strained films does not have a major effect on the concentration of vacancies, it will change the band structure in the valence band region and consequently change the electrical properties. Expanding the lattice by epitaxial growth on a substrate with a larger lattice constant like MgO will decrease the bandwidth and therefore increase the gap. This explains the lower conductivity and higher room temperature activation energies found in our films. In the models proposed by Goodenough⁸ and Mott⁹, the on-site Coulomb interaction U is assumed to open up a small energy gap in the itinerant t_{2g} band. It is assumed that overlapping tails of localized states, which are related to the disorder associated with the large number of defects in the system, are present at the edges of these Hubbard bands. In this way Mott⁹ explains why in bulk samples the conductivity vs temperature is semiconductor-like at high temperature, but is better described by a variable range hopping mechanism at low temperatures. The conductivity results for our films are consistent with this explanation. The main difference is that the resistivity and apparent activation energies of the films are much higher, and that the transition from semiconducting to metallic behavior is shifted to lower x values, i.e. from $x \approx 1$ in bulk samples to $x \approx 0.8$ in films.

V. CONCLUSIONS

We have successfully grown epitaxial VO_x films on MgO(100) substrates. Up to at least 120Å the growth is coherent and layer-by-layer-like. $^{18}O_2$ -RBS was introduced as a convenient method to determine accurately the stoichiometry of these ultrathin layers. Once the stoichiometry is known, the vacancy concentration of both vanadium and oxygen can be calculated from the time to grow one monolayer as determined from RHEED. The numbers turn out to be very similar to those for the bulk material. This implies that the formation of a high concentration of vacancies may not be directly related to an increased t_{2g} band width as a result of a vacancy induced lattice contraction. Instead we suggest that a detailed study is required to calculate the possible stabilization due to additional ligand field splittings at the low symmetry metal sites near the vacancies, as observed from XAS. Nevertheless, the decrease in direct overlap between t_{2g} orbitals and the concomitant increase of the size of the pseudo-gap between the lower and upper t_{2g} Hubbard bands is held responsible for the much larger electrical resistivity in strained VO_x films.

VI. ACKNOWLEDGEMENTS

We would like to thank D. I. Khomskii, T. T. M. Palstra and D. O. Boerma for stimulating discussions, as well as H. Bruinenberg and J. Baas for skillful technical assistance. We would like to thank A. Tanaka for the use of the code to calculate the XAS spectra. The research of M.W.H. and L.H.T. is supported by the Deutsche Forschungsgemeinschaft through SFB 608.

-
- ¹ J. B. Goodenough, *Magnetism and the Chemical Bond*, Interscience Publishers, John Wiley and Sons, New York, 1963.
 - ² W. Brückner, H. Oppermann, W. Reichelt, J. I. Terukow, F. A. Tschudnowski, and E. Wolf, *Vanadiumoxide*, Akademie-Verlag, Berlin 1983.
 - ³ N. Tsuda, K. Nasu, A. Fujimori, and K. Siratori, *Electronic Conduction in Oxides*, Springer-Verlag, 2000.
 - ⁴ M. Imada, A. Fujimori, and Y. Tokura, *Rev. Mod. Phys.* **70**, 1039 (1998).
 - ⁵ C. N. R. Rao and B. Raveau, *Transition Metal Oxides*, Wiley-VCH, New York, 1998.
 - ⁶ M. D. Banus, T. B. Reed, and A. J. Strauss, *Phys. Rev. B* **5**, 2775 (1972).
 - ⁷ M. Morinaga, and J. B. Cohen, *Acta Cryst. A* **35**, 745 (1979).
 - ⁸ J. B. Goodenough, *Phys. Rev. B* **5**, 2764 (1972).
 - ⁹ N. F. Mott, *Phyl. Mag.* **24**, 935 (1971).
 - ¹⁰ P. A. Cox, *Transition Metal Oxides*, Oxford University Press, Oxford, (1995).
 - ¹¹ A. Neckel, P. Rastl, R. Eibler, P. Weinberger, and K. Schwarz, *J. Phys. C* **9**, 579 (1976).
 - ¹² K. Kishi, K. Hirai, and T. Yamamoto, *Surf. Sci.* **290**, 309 (1993).
 - ¹³ K. Kishi, Y. Hayakawa, and K. Fujiwara, *Surf. Sci.* **356**, 171 (1996).
 - ¹⁴ K. Kishi and K. Fujiwara, *J. Electron Spectrosc. Relat. Phenom.* **85**, 123 (1997).
 - ¹⁵ T. Hartmann and H. Knozinger, *Z. Phys. Chem. (Munich)* **197**, 113 (1996).
 - ¹⁶ F. P. Leisenberger, S. Surnev, L. Vitali, M. G. Ramsey, and F. P. Netzer, *J. Vac. Sci. Technol. A* **17**, 1743 (1999).
 - ¹⁷ S. Surnev, L. Vitali, M. G. Ramsey, and F. P. Netzer, *Phys. Rev. B* **61**, 13945 (2000).
 - ¹⁸ V. E. Henrich and P. A. Cox, *The Surface Science of Metal Oxides* (Cambridge University Press, Cambridge, 1994).
 - ¹⁹ M. D. Negra, M. Sambhi, and G. Granozzi, *Surf. Sci.* **436**, 227 (1999).

- ²⁰ M. D. Negra, M. Sambi, and G. Granozzi, *Surf. Sci.* **461**, 118 (2000).
- ²¹ M. Sambi, M. D. Negra, and G. Granozzi, *Thin Solid Films* **400**, 26 (2001).
- ²² F. C. Voogt, T. Fujii, M. A. James, and T. Hibma, *Phys. Rev. B* **63**, 125409 (2001).
- ²³ M. A. James, F. C. Voogt, B. Niesen, O. C. Rogojuanu, and T. Hibma, *Surf. Sci.* **402-404**, 332 (1998).
- ²⁴ M. A. James and T. Hibma, *Surf. Sci.* **433-435**, 718 (1999).
- ²⁵ H. Schuler, S. Klimm, G. Weissmann, C. Renner, and S. Horn, *Thin Solid Films* **299**, 119 (1997).
- ²⁶ H. Schuler, G. Weissmann, C. Renner, S. Six, S. Klimm, F. Simmet, and S. Horn, *Mat. Res. Soc. Symp.Proc.*, Vol **401**, 61 (1996).
- ²⁷ H. Schuler, S. Grigoriev, and S. Horn, *Mat. Res. Soc. Symp.Proc.*, Vol **474**, 291 (1997).
- ²⁸ C. T. Chen, *Nucl. Instrum. Methods Phys. Res., Sect. A* **256**, 595 (1987).
- ²⁹ C. T. Chen and F. Sette, *Rev. Sci. Instrum.* **60**, 1616 (1989).
- ³⁰ G. Sawatzky and D. Post, *Phys. Rev. B* **20**, 1546 (1979).
- ³¹ M. Abbate, H. Pen, M. T. Czyzyk, F. M. F. de Groot, F. C. Fuggle, Y. J. Ma, C. T. Chen, F. Sette, A. Fujimori, Y. Ueda, and K. Kosuge, *J. Electron Spectros. Relat.Phenom.* **62**, 185 (1993).
- ³² F. M. F. de Groot, M. Grioni, F. C. Fuggle, J. Ghijsen, G. A. Sawatzky, and H. Petersen, *Phys. Rev. b* **40**, 5715 (1989).
- ³³ J. van Elp and Arata Tanaka, *Phys. Rev. B* **60**, 5331 (1999).
- ³⁴ S. Nakai, T. Mitsuishi, H. Sugawara, H. Maezawa, T. Matsukawa, S. Mitani, K. Yamasaki, and T. Fujikawa, *Phys. Rev. B* **36**, 9241 (1987).
- ³⁵ See review by F.M.F. de Groot, *J. Electron Spectrosc. Relat. Phenom.* **67**, 529 (1994).
- ³⁶ See review in the Theo Thole Memorial Issue, *J. Electron Spectrosc. Relat. Phenom.* **86**, 1 (1997).
- ³⁷ A. Tanaka and T. Jo, *J. Phys. Soc. Jpn.* **63**, 2788 (1994).
- ³⁸ N. Mott, *Metal-Insulator Transitions*, Taylor&Francis (1990).
- ³⁹ A. R. Brown, C. P. Jarrett, D. M. de Leeuw, and M. Matters, *Synthetic Metals*, **88**, 37-55 (1997).
- ⁴⁰ P. W. Anderson and H. Hasagawa, *Phys. Rev.* **100**, 675 (1958).
- ⁴¹ H. Erschbaumer, R. Podlucky, and A. Neckel, *J. Phys. F* **15**, L279 (1985).
- ⁴² M. D. Banus, *Mater. Res. Bull.***3**, 723 (1968).
- ⁴³ I. S. Elfimov, S. Yunoki, and G. A. Sawatzky, *Phys. Rev. Lett.* **89** 89, 216403 (2002).